Analysis of High-Frequency Common Mode Component Characteristics of Common Mode Peak Voltage Suppression Method for Indirect Matrix Converter

Haiming Liu [1,2], Linfeng Huang [3,4,*], Cheng Lin [1], Yifu Ding [2], Yun Wang [2] and Shanhu Li [3,*]

[1] School of Mechanical Engineering, Beijing Institute of Technology, Beijing 100081, China; 3220185038@bit.edu.cn (H.L.); lincheng@bit.edu.cn (C.L.)
[2] China Automotive Technology and Research Center Co., Ltd., Tianjin 300300, China; dingyifu@catarc.ac.cn (Y.D.); wangyun@catarc.ac.cn (Y.W.)
[3] State Key Laboratory of Reliability and Intelligence of Electrical Equipment, Hebei University of Technology, Tianjin 300130, China
[4] CRRC Zhuzhou Electric Locomotive Research Institute, Zhuzhou 412001, China
* Correspondence: 201931403029@stu.hebut.edu.cn (L.H.); shanhuli@hebut.edu.cn (S.L.)

Abstract: A variety of modulation strategies for suppressing output common-mode voltage (CMV) of indirect matrix converters (IMC) have been proposed, but most of them mainly reduce the peak of CMV by 42.3%. The frequency-domain characteristics of CMV have not been deeply analyzed. In order to improve the theory of frequency-domain characteristics of output common-mode voltage of IMC, this paper proposed a common-mode frequency domain analysis of five common-mode voltage peak suppression modulation methods for IMC. The common-mode voltage spectrum corresponding to the five modulation methods is obtained by the triple Fourier series, and the variation laws of the output common-mode components of the five modulation methods under different modulation indexes are compared and analyzed. By comparing and analyzing the low-frequency amplitude characteristics and high-frequency amplitude characteristics of five modulation methods, the suppression performance of the five modulation methods is evaluated. Finally, experiments verify the correctness of the theoretical analysis of the frequency domain characteristics of the output common-mode voltage of the indirect matrix converter.

Keywords: indirect matrix converter (IMC); common-mode components; spectrum analysis; triple Fourier series; voltage transfer ratio (VTR)

1. Introduction

The indirect Matrix Converter (IMC) has a wide range of application prospects in new energy power generation systems and AC transmission fields due to its sinusoidal input/output current waveform, adjustable input power factor, compact structure, and other excellent advantages [1]. However, the output voltage of PWM modulated IMC contains huge amounts of common-mode components. The high-frequency and high-magnitude common-mode voltage (CMV) will generate the bearing current [2], destroy the winding insulation and shorten the operating life of an ac motor [3]. At the same time, high-frequency CMV will cause electromagnetic interference to the surrounding equipment [4] and affect the reliable operation and electromagnetic compatibility of the motor drive system, which affects the operating performance of the motor drive system [5].

In order to improve the output quality of IMC, the method of suppressing CMV can be divided into hardware compensation and software compensation. Hardware compensation includes adding a filter and CMV suppressor at the output end of IMC, which increases the weight and volume of the system and reduces the power density of the system [6,7]. Software compensation represents reasonable modulation strategy optimization. There has been much literature that analyzes and suppresses CMV. In literatures [8–13], the peak

magnitude of CMV is reduced by changing vector selection in the rectifier or inverter stage of IMC. However, these methods do not consider suppressing high-frequency common-mode components in output voltage. The existing modulation methods mainly focus on the suppression of the peak magnitude of CMV, and there are few studies on the suppression of common-mode components. The harm of common-mode voltage to the motor system is not only related to the peak magnitude of CMV, but also the high amplitude of common-mode components, and the high frequency of common-mode components also have a great impact on the motor system, so suppression of common-mode components is necessary.

In order to suppress common-mode components of IMC, it is necessary to deeply analyze the frequency domain characteristics of CMV and quantitatively analyze the variation law of common-mode components. At present, one of the commonly used quantitative analysis methods for output components is FFT analysis. However, when signals are sampled and windowed by FFT analysis, it brings problems such as frequency leakage and aliasing, which results in FFT analysis being inaccurate [14]. Another analysis method is to mathematically model the output waveform and calculate output components through mathematical derivation. In literatures [15–18], the harmonic analysis of different topology converters are derived from the double Fourier series. Because the matrix converter output waveform is related to the input frequency, output frequency, and carrier frequency, the output spectrum results obtained by the double Fourier series are inaccurate. In the literature [19,20], the triple Fourier series is used to mathematically model the output voltage waveforms of direct matrix converter and ultra-sparse matrix converter in the traditional space vector modulation method; obtain output voltage harmonic spectrum, and analyze the variation laws of output voltage harmonic component. However, the existing research has not yet deeply analyzed the variation laws of common-mode components of different modulation methods of IMC, and in order to better suppress the common-mode components of IMC, it is necessary to further improve the theoretical study of the frequency domain characteristics of CMV of IMC.

In this paper, the influence and suppression methods of the output common-mode voltage of the indirect matrix converter are introduced, and several methods of frequency domain analysis of the output component are simply described in Section 1. In Section 2, CMV of five modulation methods are triple-modeled, spectrums of CMV are obtained, and the frequency domain characteristics of CMV are analyzed. In Section 3, compares the suppression abilities of five modulation methods on common-mode components, and considering the effects of voltage transmission ratio (VTR) on the common-mode components at the same time, it can be seen that the modulation method 1, in which the inverter stage uses four effective vectors has the strongest ability to suppress common-mode voltage among five modulation methods; In Section 4, the correctness of the theoretical analysis is verified by experiments. Finally, the frequency domain characteristics of IMC output common-mode voltage of five modulation methods are summarized in Section 5.

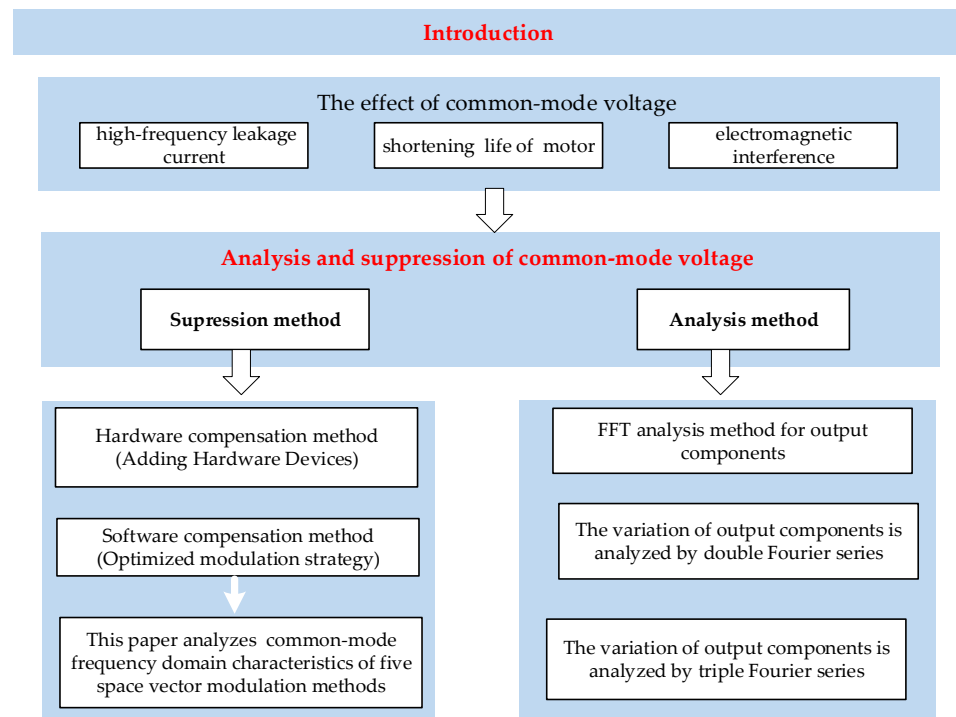The main contributions of the introduction section are shown in Figure 1.

Figure 1. Contribution block diagram of introduction.

2. Triple Fourier Modeling of Common-Mode Voltage of Space Vector Modulation

2.1. Traditional Space Vector Modulation

The topology of IMC is shown in Figure 2, which is divided into two parts: the rectifier stage and the inverter stage. The sector division of the rectifier stage is shown in Figure 3.
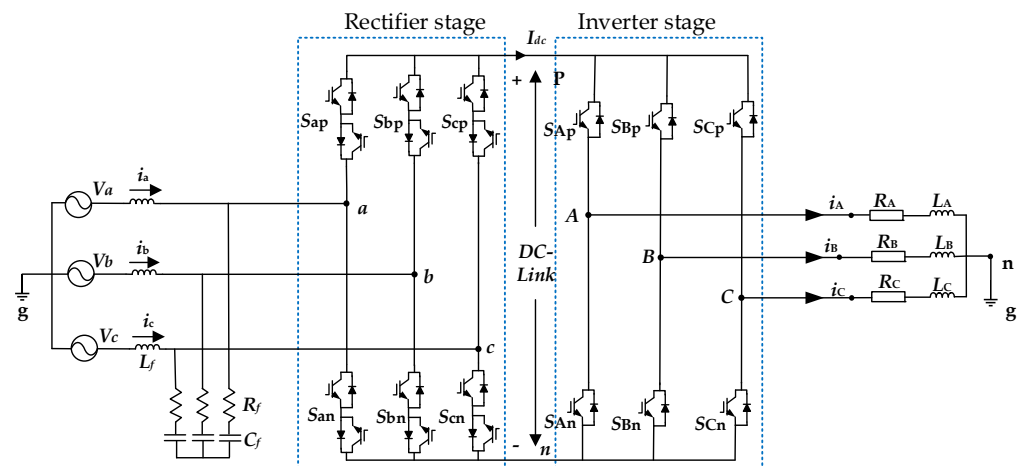

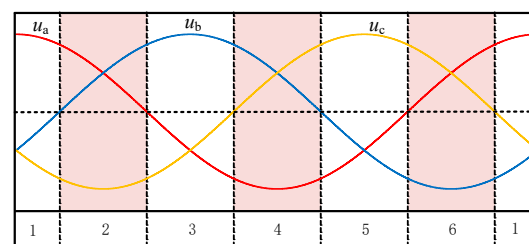**Figure 2.** Topology of IMC.

Figure 3. Sector of rectifier stage.

The three-phase input voltage u_a, u_b and u_c are

$$\begin{cases} u_a = V_{in} \cos(\omega_{in} t) \\ u_b = V_{in} \cos(\omega_{in} t - 2\pi/3) \\ u_c = V_{in} \cos(\omega_{in} t + 2\pi/3) \end{cases} \tag{1}$$

where V_{in} is the input voltage amplitude, $\omega_{in} = 2\pi f_{in}$, ω_{in} is the input angle frequency, and f_{in} is the input frequency.

The traditional space vector modulation principle of IMC is shown in Figure 4; the rectifier stage modulation vectors contain six effective current vectors and three zero current vectors. The reference input current vector $\boldsymbol{I}_{ref}$ is synthesized by two adjacent effective current vectors, $\boldsymbol{I}_\delta$ and $\boldsymbol{I}_\gamma$. The inverter stage modulation vectors contain six effective voltage vectors and two zero voltage vectors. The reference output voltage vector $\boldsymbol{V}_{ref}$ is synthesized by two adjacent effective voltage vectors, $\boldsymbol{V}_\alpha$, $\boldsymbol{V}_\beta$ and two zero voltage vectors, $\boldsymbol{V}_0$ and $\boldsymbol{V}_7$. During modulation, the IMC generates common-mode voltage u_{ng} between the load neutral point n and the power supply location g, and the calculation expression of u_{ng} is

$$u_{ng} = \left(u_{Ag} + u_{Bg} + u_{Cg}\right)/3 \tag{2}$$

where u_{Ag}, u_{Bg} and u_{Cg} are three-phase output voltages.

(a) Rectifier stage modulation   (b) Inverter stage modulation
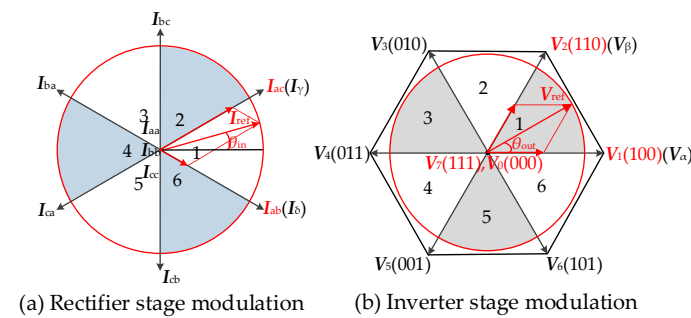
Figure 4. Space Vector Modulation Principle of IMC.

According to the traditional SVM principle, the peaks of common-mode voltage under the action of modulation vectors of different rectifier stages and inverter stages are shown in Table 1.

Table 1. Common-mode voltage under different vectors.

k_{in}	Current Vectors	Voltage Vectors	Common-Mode Voltage
1, 3, 5	I_δ I_γ	$V_1 \sim V_6$ V_7 (111) V_0 (000)	$0.577V_{in}$ V_{in} $0.866V_{in}$
2, 4, 6	I_δ I_γ	$V_1 \sim V_6$ V_0 (000) V_7 (111)	$0.577V_{in}$ V_{in} $0.866V_{in}$

From Table 1, it can be seen that when the inverter stage adopts the zero voltage vector, the maximum value of common-mode voltage is V_{in}, and when the inverter stage adopts the effective voltage vector, the maximum value of common-mode voltage is $0.577V_{in}$. Therefore, most of the existing improved modulation methods reduce the peak of CMV without using the zero voltage vector.

2.2. Modulation Methods to Suppress 42.3% Common-Mode Voltage Peaks

In this paper, five modulation methods that suppress the 42.3% peak of CMV are used as research objects to analyze the frequency domain characteristics of the CMV. The five

modulation methods do not use zero voltage vectors in the inverter stage. The following describes each of the five modulation methods.

2.2.1. Method 1

The vector arrangement of method 1 and the synthesis waveform of common-mode voltage u_{ng} are shown in Figure 5. The reference input current vector I_{ref} of the rectifier stage is synthesized from two adjacent effective current vectors. The inverter stage uses two effective voltage vectors opposite to each other instead of the zero voltage vector, and the reference output voltage vector V_{ref} is synthesized by four adjacent effective voltage vectors. From the vector synthesis principle and duty cycle calculation, it can be seen that the voltage transmission ratio m (m is the ratio of V_{ref}/V_{in}) range of method 1 is (0, 0.866).
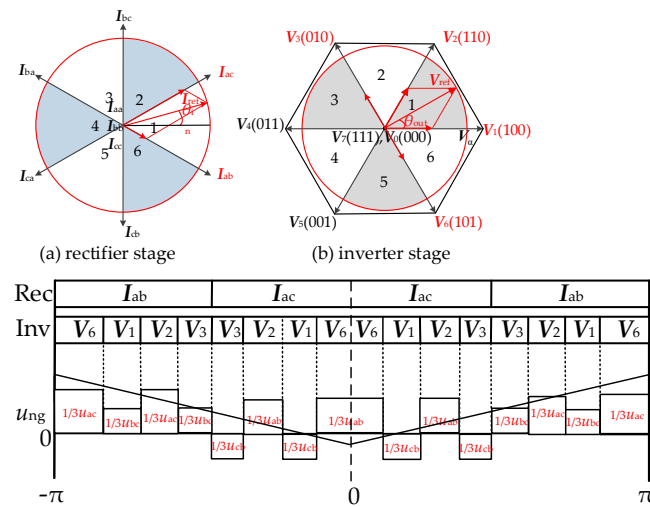

Figure 5. Modulation principle and vector distribution of method 1.

2.2.2. Method 2

The vector arrangement of method 2 and the synthesis waveform of the common-mode voltage u_{ng} are shown in Figure 6. Method 2 re-divides into 6 sectors of the inverter stage. In the new sector of the inverter stage, the reference output voltage vector V_{ref} is synthesized by three adjacent effective voltage vectors, and the rectifier stage modulation principle is the same as method 1. The voltage transmission ratio range of method 2 is (0.577, 0.866).
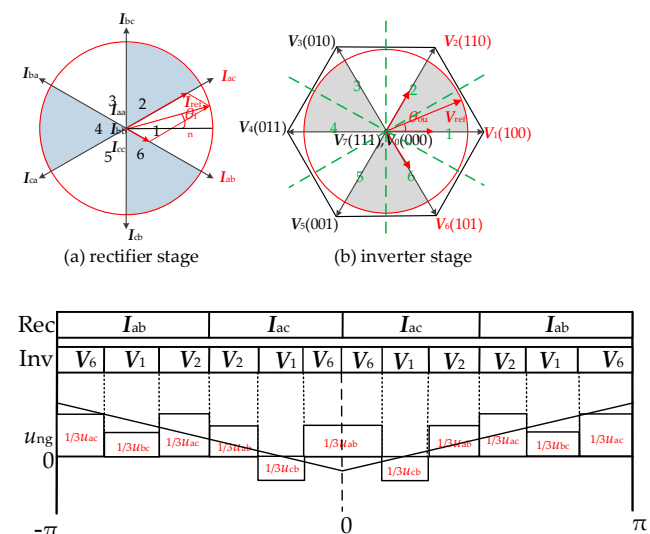

Figure 6. Modulation principle and vector distribution of method 2.

2.2.3. Method 3

The vector arrangement of method 3 and the synthesis waveform of the common-mode voltage u_{ng} are shown in Figure 7. Method 3 re-divides into six sectors of the rectifier stage; the reference input current vector I_{ref} is synthesized by three adjacent effective current vectors, and the inverter stage reference output voltage vector V_{ref} is synthesized by two adjacent effective voltage vectors. The voltage transmission ratio range of method 3 is (0.577, 0.866).
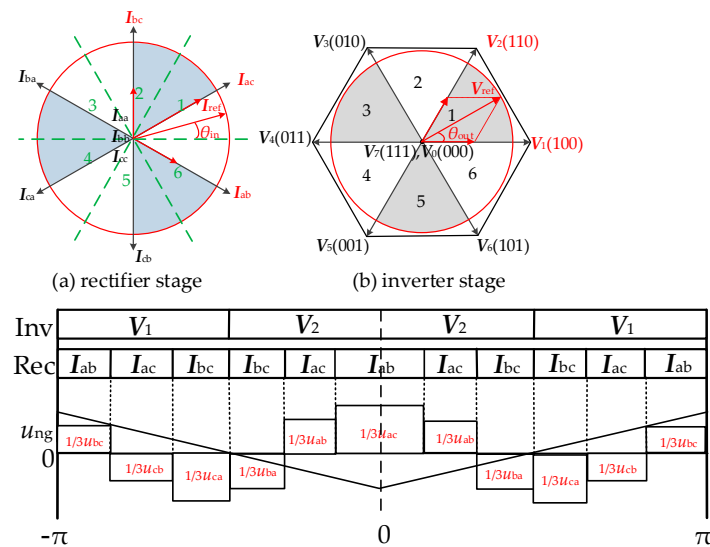

Figure 7. Modulation principle and vector distribution of method 3.

2.2.4. Method 4

The vector arrangement of method 4 and the synthesis waveform of the common-mode voltage u_{ng} is shown in Figure 8. Method 4 rectifier sector division is the same as method 3, and the reference input current vector I_{ref} is synthesis by two effective current vectors are a difference of 120° and zero current vectors, where the selection of the zero vector of the rectifier stage needs to ensure that the intermediate DC bus and the absolute minimum input voltage are connected. The inverter stage reference voltage vector V_{ref} is synthesized by two adjacent effective voltage vectors. The voltage transfer ratio range of method 4 is (0, 0.5).
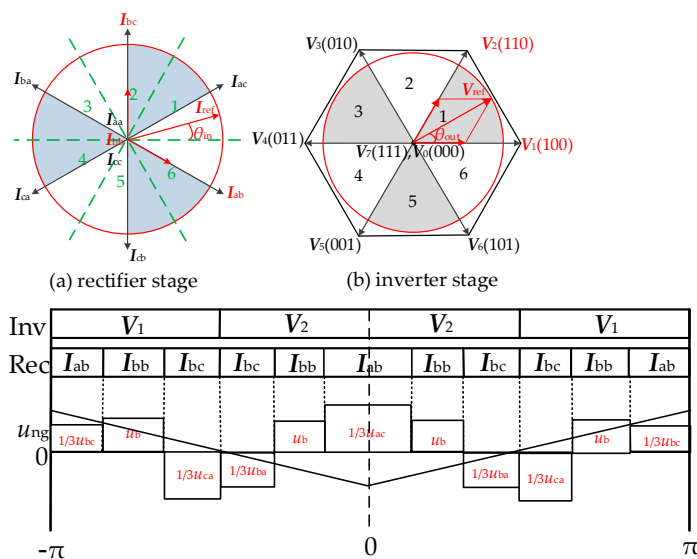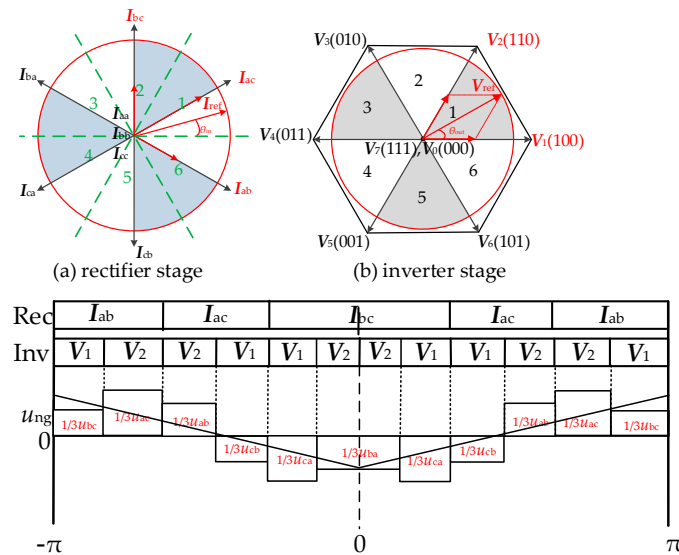

Figure 8. Modulation principle and vector distribution of method 4.

2.2.5. Method 5

The vector arrangement of method 5 and the synthesis waveform of the common-mode voltage u_{ng} are shown in Figure 9. The rectifier stage reference input current vector I_{ref} is synthesized by three adjacent effective current vectors, and the inverter stage reference output voltage vector V_{ref} is synthesized by two adjacent effective voltage vectors. The voltage transfer ratio range of method 4 is (0.677, 0.866).

(a) rectifier stage　　　　　　(b) inverter stage

Figure 9. Modulation principle and vector distribution of method 5.

2.3. Triple Fourier Modeling of Output Common-Mode Voltages

Because output waveforms of IMC are related to the input frequency, output frequency, and carrier frequency, the three frequencies are independent of each other. To analyze frequency domain characteristics of CMV and evaluate the ability of five modulation methods to reduce common-mode voltage, the common-mode voltage is modeled based on the triple Fourier series and obtained spectrums of CMV in this paper.

The expression for symmetric triangular carrier $c(\theta_c)$ of modulation methods is

$$c(\theta_c) = \frac{1}{\pi}\arccos[\cos(\theta_c)] \tag{3}$$

where $\theta_c = 2\pi f_c t$, f_c is the carrier frequency.

According to vector arrangements of modulation methods and synthesis waveform of CMV, common-mode voltage u_{ng} is a time-varying periodic function and is segmented smoothly on a carrier cycle. Therefore common-mode voltage $u_{ng}(\theta_c,\theta_{in},\theta_{out})$ satisfies the condition of Fourier expansion. The common-mode voltage is expanded by a Fourier series, and the expression $u_{ng}(\theta_c,\theta_{in},\theta_{out})$ is

$$u_{ng}(\theta_c, \theta_{in}, \theta_{out}) = \sum_{k=-\infty}^{+\infty}\sum_{p=-\infty}^{+\infty}\sum_{q=-\infty}^{+\infty} F_{k,p,q} \cdot e^{j(k\theta_c + p\theta_{in} + q\theta_{out})} \tag{4}$$

The triple Fourier coefficient $F_{k,p,q}$ of common-mode voltage is

$$\begin{aligned} F_{k,p,q} &= \frac{A_{k,p,q} - jB_{k,p,q}}{2} \\ &= \frac{1}{8\pi^3}\int_0^{2\pi}\int_0^{2\pi}\int_0^{2\pi}\left[u_{ng}(\theta_c, \theta_{in}, \theta_{out}) \cdot e^{-jk\theta_c}e^{-jp\theta_{in}}e^{-jq\theta_{out}}\right]d\theta_c d\theta_{in} d\theta_{out} \end{aligned} \tag{5}$$

where k, p, and q are integers, $A_{k,p,q}$, and $B_{k,p,q}$ are the real and imaginary parts of the triple Fourier coefficients, respectively.

The amplitudes of common-mode components of frequency $kf_c \pm pf_{in} \pm qf_{out}$ are

$$V_{k,p,q} = 2\left|F_{k,p,q}\right| = \sqrt{A^2_{k,p,q} + B^2_{k,p,q}} \tag{6}$$

Taking the first sector of the rectifier stage and the inverter stage as an example, Figures 5–9 shows a synthetic waveform of CMV under a triangular carrier of five modulation methods. Similarly, according to the principles of modulation methods, the synthetic waveform of common-mode voltage of other sectors can be known. Bring u_{ng} and the common-mode voltage switching time into Equation (5), calculate the triple Fourier coefficient of common-mode voltage, and the amplitudes of output common-mode components are obtained according to Equation (6). The common-mode voltage is normalized, and the Per-unit value h_{com} of common-mode components are

$$h_{com} = 2\left|F_{k,p,q}\right| / V_{in} \tag{7}$$

3. Theoretical Analysis and Comparison of Common-Mode Components

The voltage transfer ratio m of five modulation methods is shown in Table 2. Compared with traditional SVM, the voltage transfer ratio of method 1 is not affected. Furthermore, method 4 can only operate in the low voltage transmission ratio range, and method 2, method 3, and method 5 can only operate in the high voltage transmission ratio range.

Table 2. Voltage transfer ratio for different modulation methods.

	Method 1	Method 2	Method 3	Method 4	Method 5
m	0~0.866	0.577~0.866	0.577~0.866	0~0.500	0.667~0.866

Because the VTR of five modulation methods is inconsistent, in order to quantitatively analyze variations of common-mode components of different modulation methods and evaluate suppression abilities of different modulation methods on the common-mode components, the frequency domain characteristics of common-mode components corresponding to different modulation methods in high VTR range and low VTR range are studied.

3.1. Analysis and Comparison of Common-Mode Components in Low VTR Range

Firstly, the frequency domain characteristics of the common-mode components under the low voltage transmission ratio range (0, 0.5) are analyzed. As can be seen from Table 2, method 1 and method 4 operate in the range (0, 0.5). When the input voltage V_{in} is 70.7 V, input frequency f_{in} is 50 Hz, output frequency f_{out} is 70 Hz, and carrier frequency f_c is 5 kHz, common-mode voltage spectrums of method 1 and method 4 at $m = 0.3$ can be obtained by calculation. The common-mode components are normalized based on input voltage V_{in}, and obtain Per-unit value of common-mode components, as shown in Figure 10.
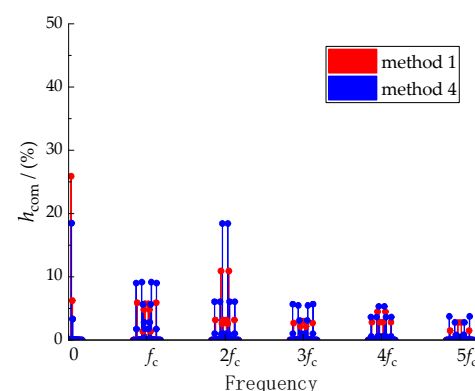
Figure 10. Spectrum of the common-mode components at $m = 0.3$.

As can be seen from Figure 10, the common-mode components are greatest in the $2f_c$ band. In order to more clearly analyze the frequency domain characteristics of common-mode voltage in different frequency bands of method 1 and method 4, common-mode components of different frequency bands are partially amplified, as shown in Figure 11. Extracted main common-mode components from the spectrum of CMV as shown in Table 3.
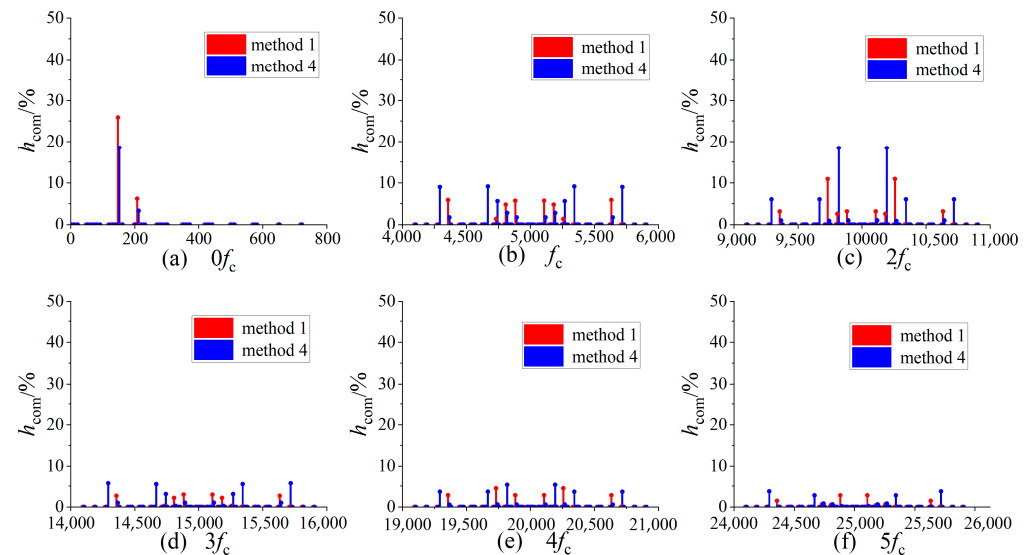

Figure 11. Partial enlargement of Figure 10.

Table 3. Per-unit value of common-mode components at $m = 0.3$.

$kf_c \pm pf_{in} \pm qf_{out}$	h_{com} (%)	
	Method 1	**Method 4**
$3f_{out}$	6.20	4.29
$3f_{in}$	25.91	18.56
$f_c \pm 3f_{out}$	0.37	5.36
$f_c \pm 3f_{in}$	4.88	0.43
$f_c \pm 6f_{in} \pm 3f_{out}$	5.64	1.46
$2f_c \pm 3f_{out}$	10.21	0.18
$2f_c \pm 3f_{in}$	2.58	18.34
$3f_c \pm 3f_{out}$	0.07	2.83
$3f_c \pm 6f_{in} \pm 3f_{out}$	2.96	0.95
$4f_c \pm 3f_{out}$	4.50	0.60
$4f_c \pm 3f_{in}$	0.05	5.47
$5f_c \pm 3f_{out}$	0.18	0.78
$5f_c \pm 6f_{in} \pm 3f_{out}$	1.77	0.01

From Table 3 and Figure 11, it can be seen that $3f_{in}$ is the main common-mode component in the low-frequency band, the amplitude of $3f_{in}$ of method 1 is 25.91%, and the amplitude of $3f_{in}$ of method 4 is 18.56%. From Figure 11b, it can be seen that common-mode components of method 4 in the f_c frequency band are greater than that of method 1, the maximum amplitude of common-mode components of method 1 is 5.64%, and the maximum amplitude of common-mode components of method 4 is 9.14%. From Figure 11c, the maximum common-mode components of method 1 are 10.72%, which is obtained at frequency $2f_c \pm 3f_{out}$. The maximum common-mode components of method 4 are 18.43%, and the maximum common-mode components of method 4 are obtained at frequency $2f_c \pm 3f_{in}$. As frequency increases, the main common-mode components of $3f_c$, $4f_c$, and $5f_c$ frequency bands gradually decrease. Extracted the maximum common-mode components of different frequency bands from method 1 and method 4 are shown in Figure 12.
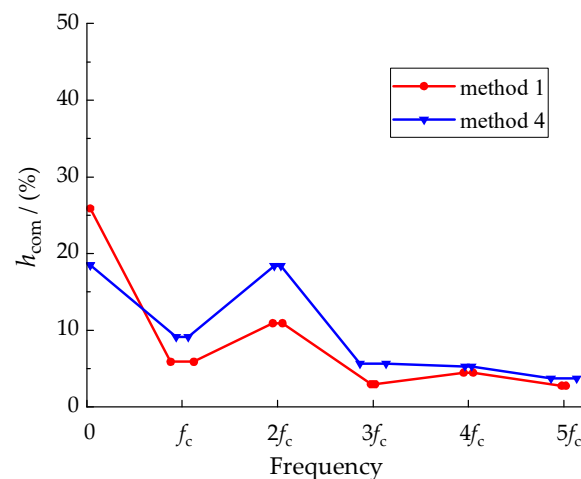
Figure 12. Maximum peak values of common-mode components at different frequency bands.

As can be seen from Figure 12, the common-mode components of method 1 and method 4 in the low-frequency band are larger than high frequency band. In the high-frequency band, in addition to the common-mode components in the $2f_c$ frequency band, the common-mode components of method 1 and method 4 show a decreasing amplitude trend as the frequency increases. In the low-frequency band, the maximum common mode amplitude of method 1 is greater than method 4. In the high-frequency band, the maximum common-mode components amplitude of method 4 are greater than method 1. Above the $3f_c$ frequency band, the difference between the amplitude of the maximum common-mode components of method 1 and method 4 is small.

When $m = 0.3$, it can be seen that the amplitude of high-frequency common-mode components of method 1 is smaller than that of method 4 by analyzing the frequency domain characteristics of the common-mode voltage of method 1 and method 4. This shows that the high-frequency characteristics and suppression ability of output common-mode components of method 1 are better than those of method 4.

3.2. Analysis and Comparison of Common-Mode Components in High VTR Range

As can be seen from Table 2, in addition to method 4, the other four modulation methods can operate in the high VTR range. When input voltage V_{in} is 70.7 V, input frequency f_{in} is 50 Hz, output frequency f_{out} is 70 Hz, and carrier frequency f_c is 5 kHz, the common-mode voltage spectrums of method 1, method 2, method 3, and method 5 at $m = 0.7$ can be obtained by calculation. The common-mode components are normalized based on input voltage V_{in}, and obtain Per-unit value of common-mode components, as shown in Figure 13.
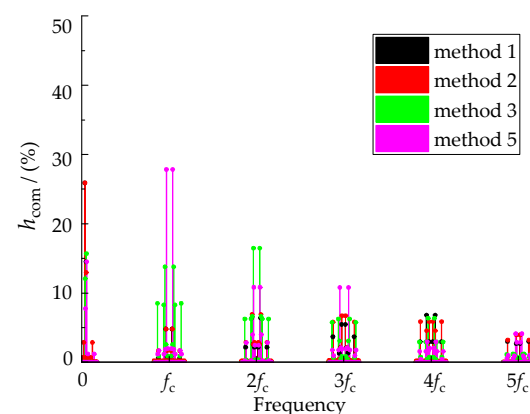
Figure 13. Spectrum of the common-mode components at $m = 0.7$.

Figure 13 lists the main common-mode components of method 1, method 2, method 3, and method 5 at $0\sim5f_c$ frequency bands. From Figure 13, it can be seen that common-mode components of the high-frequency band decrease with frequency increase gradually. In order to more clearly analyze the variation of common-mode components of four modulation methods in different frequency bands, common-mode components of different frequency bands are partially amplified, as shown in Figure 14. Extracted main common-mode components from the spectrum as shown in Table 4.
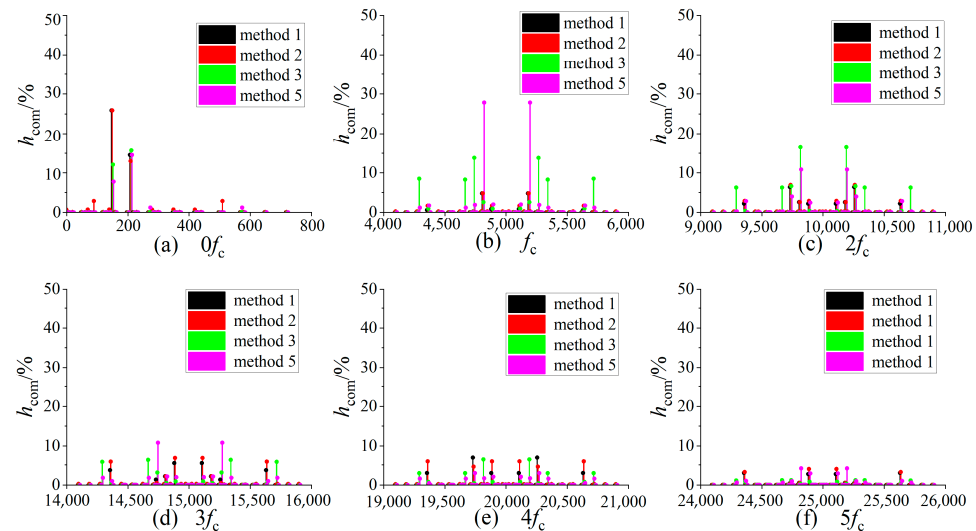

Figure 14. Partial enlargement of Figure 13.

Table 4. Per-unit value of common-mode components at $m = 0.7$.

$kf_c \pm pf_{in} \pm qf_{out}$	h_{com} (%)			
	Method 1	**Method 2**	**Method 3**	**Method 5**
$3f_{out}$	14.54	13.35	15.70	14.50
$3f_{in}$	25.95	25.94	12.14	8.01
$f_c \pm 3f_{out}$	0.14	0.17	13.72	1.30
$f_c \pm 3f_{in}$	4.99	4.96	0.22	27.82
$f_c \pm 6f_{in} \pm 3f_{out}$	0.88	1.98	0.87	2.35
$2f_c \pm 3f_{out}$	5.72	6.65	8.48	4.26
$2f_c \pm 3f_{in}$	2.64	2.65	16.95	10.98
$3f_c \pm 3f_{out}$	0.46	0.22	3.22	10.74
$3f_c \pm 6f_{in} \pm 3f_{out}$	4.40	6.10	0.69	1.03
$4f_c \pm 3f_{out}$	6.61	4.82	0.65	3.25
$4f_c \pm 3f_{in}$	0.18	0.19	6.82	1.82
$5f_c \pm 3f_{out}$	0.19	0.20	1.32	1.03
$5f_c \pm 6f_{in} \pm 3f_{out}$	3.05	3.12	0.85	1.39

From Figure 14 and Table 4, it can be seen that the maximum common-mode components of method 1 and method 2 in the low-frequency band are 25.91%, and the maximum common-mode component of method 3 and method 5 in the low-frequency band are 15.7% and 14.5%, respectively. This shows that the suppression ability of method 1 and method 2 is worse than that of method 3 and method 5 at the low-frequency band. In the f_c frequency band, the maximum common-mode components amplitude of method 1 and method 2 are 4.9%, generated at the $f_c \pm 3f_{in}$. The maximum common-mode components amplitude of method 3 is 13.7%, generated at $f_c \pm 3f_{out}$, and the maximum common-mode components amplitude of method 5 is 27.8%, generated at $f_c \pm 3f_{in}$. It shows that the suppression ability of method 1 and method 2 is better than that of method 3 and method 5 at the f_c frequency band. In the $2f_c$ frequency band, neither method 1 nor method 2 has a maximum peak of

common-mode components exceeding 10%. The maximum common-mode components amplitude is 16.85% at the $2f_c$ frequency band, which is generated by method 3 at $2f_c \pm 3f_{in}$. The maximum common-mode component is generated by method 5 at $3f_c \pm 3f_{out}$, and the amplitude of the maximum common-mode component is 10.7% at the $3f_c$ frequency band. The common-mode components of other modulation methods are small and symmetrically distributed around the switching frequency band. The common-mode components in the frequency bands of $4f_c$ and $5f_c$ are small, and the differences between the common-mode components of different modulation methods are not obvious.

Extracted the maximum common-mode components of method 1, method 2, method 3, and method 5 at different frequency bands, as shown in Figure 15.
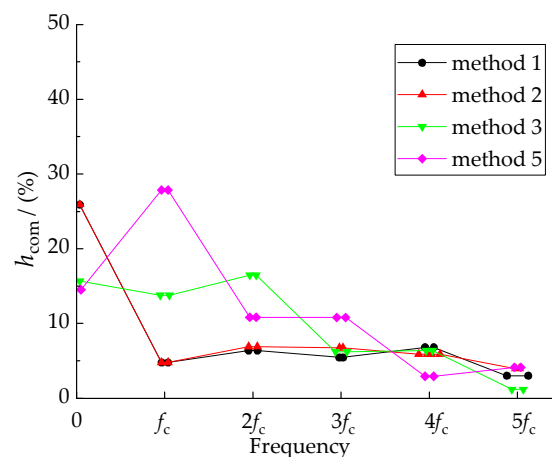
Figure 15. Maximum peak values of common-mode components at different frequency bands.

As can be seen from Figure 15, the maximum values of method 5 in the low-frequency band are the smallest, and the maximum value of method 1 and method 2 is the largest. In the f_c frequency band and $2f_c$ frequency band, the common-mode voltage maximum values of method 1 and method 2 are the smallest, method 5 is the largest at the f_c frequency band, and method 3 is the largest at the $2f_c$ frequency band. In frequency bands of $3f_c$, $4f_c$, and $5f_c$, the maximum values corresponding to four modulation methods is close. As can be seen from Figure 15, the polylines of method 1 and method 2 are basically coincident, and only in high-frequency bands, which shows that the variation law of the maximum common-mode components of the two methods is basically the same. The amplitude corresponding to method 1 is slightly smaller than that of method 2.

When $m = 0.7$, comparing the frequency domain characteristics of common-mode components of the four modulation methods, it can be seen that method 1 has the strongest ability to suppress high-frequency common-mode components.

3.3. Frequency Domain Characteristic Analysis of Common-Mode Components of Voltage Transmission Ratio

The frequency-domain characteristics of common-mode components have been analyzed at $m = 0.3$ and $m = 0.7$. In order to further analyze the influence of m on the frequency-domain characteristics of common-mode voltage of five modulation methods, the spectrum of main common-mode components in different frequency bands varying with m is obtained by calculating common-mode components corresponding to different modulation methods under different m, as shown in Figure 16.
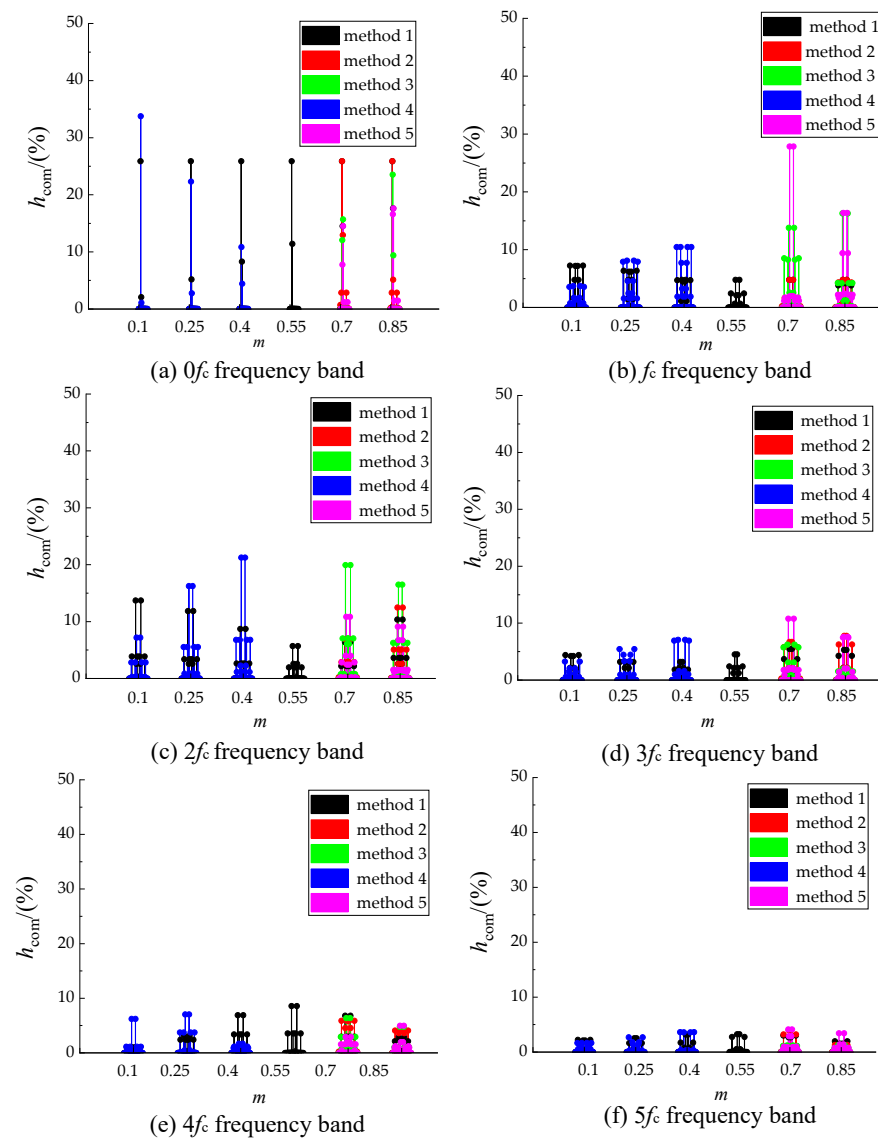
Figure 16. Spectrum of common-mode components with *m*.

Figure 16a shows the spectrum of common-mode components in the low-frequency-band of different modulation methods with *m*. It can be seen that the amplitude of low-frequency common-mode component $3f_{in}$ of method 1 is the same as method 2, and *m* has no effect on $3f_{in}$ of method 1 and method 2. The amplitude of low-frequency common-mode component $3f_{in}$ corresponding to method 4 decreases with the increase in *m*. The component $3f_{in}$ corresponding to method 3 and method 5 increases with the increase in *m*. The component $3f_{out}$ of method 2 decreases with the increase in *m*, and the component $3f_{out}$ of other methods increases with the increase in *m*.

From Figure 16b, it can be seen that common-mode components of method 1 and method 5 in the f_c frequency band are inversely proportional to *m*, and common-mode components of method 2 and method 4 are proportional to *m* in the f_c frequency band. In Figure 16c, common-mode components of method 2 and method 4 in the $2f_c$ frequency band increases with the increase in voltage transmission ratio *m*, and common-mode components of method 3 and method 5 in the $2f_c$ frequency band decrease with the increase in voltage transmission ratio *m*, and common-mode components of method 1 decreases first and then increases with the increase in voltage transmission ratio *m* in the $2f_c$ frequency band. Comparing Figures 16c and 16d, it can be seen that the variation law of common-mode components with *m* in the $3f_c$ frequency band of different modulation methods is basically

the same as that in the $2f_c$ frequency band. In Figure 16e,f, amplitudes of common-mode components in the $4f_c$ frequency band and $5f_c$ frequency band are small, and change is not obviously affected by m.

The common-mode components of five modulation methods under the same voltage transmission ratio can be seen in Figure 16. Except that when the voltage transmission ratio is 0.1, the common-mode components of method 1 in $f_c \sim 3f_c$ are greater than that of method 4. When the voltage transmission ratio is other values, comparing high-frequency common-mode components of different modulation methods, high-frequency common-mode components of method 1 can maintain a smaller amplitude, indicating that method 1 has the best suppression effect on high-frequency common-mode components.

4. Experimental Analysis and Validation

In order to verify the correctness of the theoretical analysis in this paper, a set of IMC experimental prototypes was built, as shown in Figure 17, and the experimental parameters are shown in Table 5.
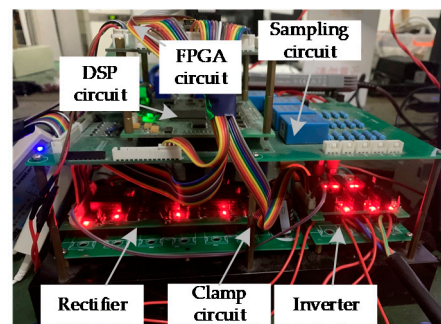

**Figure 17.** Laboratory prototype of the IMC.

Table 5. Experimental parameters.

Parameters	Value
Input voltage V_{in}	70.7 V
Input frequency f_{in}	50 Hz
Input filter parameters R_f-L_f-C_f	20 Ω/1.7 mH/10 μF
Switching frequency f_c	5 kHz
Output load R/L	20 Ω/10 mH
Output frequency f_{out}	70 Hz

When voltage transmission ratio $m = 0.3$, experimental waveforms and FFT spectrums of the common-mode voltage of methods 1 and method 4 are shown in Figure 18; When voltage transmission ratio $m = 0.7$, experimental waveforms and FFT spectrums of the common-mode voltage of methods 1, method 2, method 3 and method 5 are shown in Figure 19.

Figures 18 and 19 show experimental waveforms and FFT analysis spectrums of CMV of different modulation methods. In order to quantitatively analyze frequency domain characteristics of CMV, the main common-mode components are extracted from spectrums of CMV, and common-mode components corresponding to low transmission ratio $m = 0.3$ and high transmission ratio $m = 0.7$ are shown in Tables 6 and 7, respectively.
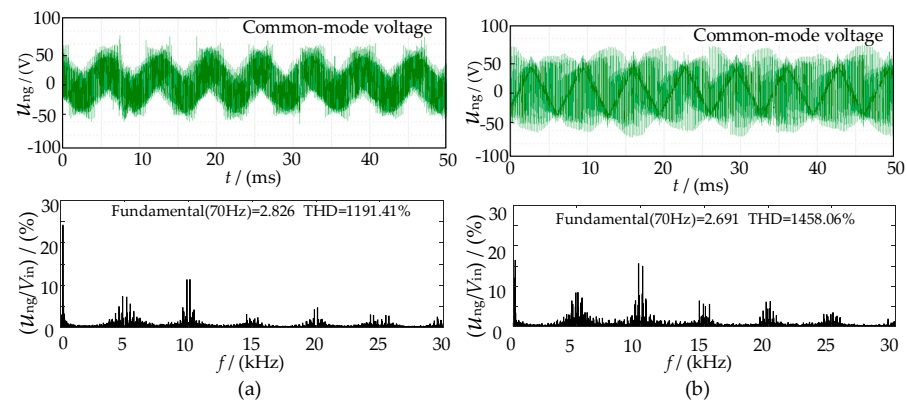
Figure 18. Experimental waveforms and FFT of CMV at $m = 0.3$ (**a**) method 1; (**b**) method 4.
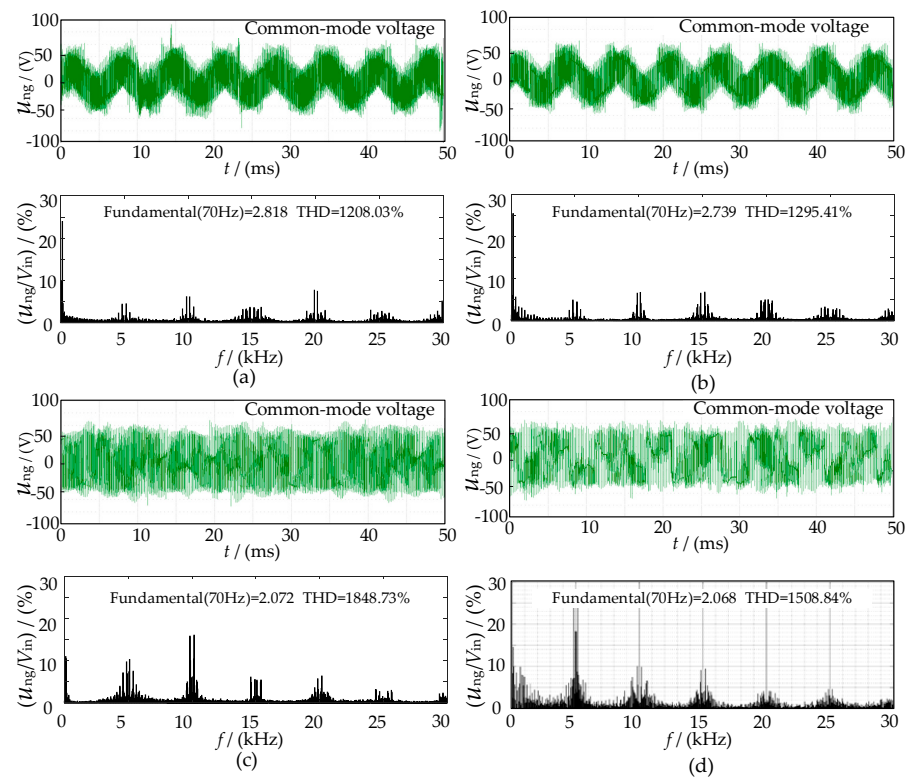
Figure 19. Experimental waveforms and FFT of CMV at $m = 0.7$ (**a**) method 1; (**b**) method 2; (**c**) method 3; (**d**) method 5.

From Figure 18 and Table 6, when $m = 0.3$, it can be seen that the amplitude of $3f_{in}$ of method 1 is 26.29%, and the amplitude of $3f_{in}$ of method 4 is 18.59%. The amplitude of common-mode components of method 4 is slightly greater than that of method 1 in the f_c frequency band; In the $2f_c$ frequency band, the maximum common-mode components of method 1 is 10.72%, and the maximum common-mode component generated by method 4 is 15.43%. Above $3f_c$ frequency, the amplitudes of common-mode components of method 1 and method 2 are similar and there are no obvious differences.

From Figure 19 and Table 7, when $m = 0.7$, it can be seen that the larger common-mode components of method 1 and method 2 are mainly concentrated in the low-frequency-band, the main common-mode components of method 5 are concentrated in the f_c frequency band, and the main common-mode components of method 3 are concentrated in the $2f_c$ frequency band. The maximum common-mode components of method 1, method 2, method 3, and method 5 in the high-frequency band are 6.6%, 6.9%, 17.2%, and 26.8%, respectively. This

shows that method 1 has the strongest ability to suppress high-frequency common-mode components when $m = 0.7$.

Table 6. Per-unit value of common-mode components of experimental waveform at $m = 0.3$.

$kf_c \pm pf_{in} \pm qf_{out}$	h_{com} (%)	
	Method 1	**Method 4**
$3f_{out}$	6.01	5.83
$3f_{in}$	26.29	18.59
$f_c \pm 3f_{out}$	0.68	5.09
$f_c \pm 3f_{in}$	5.20	0.58
$f_c \pm 6f_{in} \pm 3f_{out}$	6.46	1.91
$2f_c \pm 3f_{out}$	10.72	0.09
$2f_c \pm 3f_{in}$	3.03	15.43
$3f_c \pm 3f_{out}$	0.27	2.91
$3f_c \pm 6f_{in} \pm 3f_{out}$	2.86	1.14
$4f_c \pm 3f_{out}$	4.88	1.38
$4f_c \pm 3f_{in}$	0.36	6.10
$5f_c \pm 3f_{out}$	0.51	0.90
$5f_c \pm 6f_{in} \pm 3f_{out}$	1.42	0.17

Table 7. Per-unit value of common-mode components of experimental waveform at $m = 0.7$.

$kf_c \pm pf_{in} \pm qf_{out}$	h_{com} (%)			
	Method 1	**Method 2**	**Method 3**	**Method 5**
$3f_{out}$	13.53	13.30	13.43	11.45
$3f_{in}$	25.72	26.03	11.96	7.92
$f_c \pm 3f_{out}$	0.83	0.25	12.5	1.05
$f_c \pm 3f_{in}$	4.85	4.85	0.44	26.82
$f_c \pm 6f_{in} \pm 3f_{out}$	0.85	1.68	1.26	2.15
$2f_c \pm 3f_{out}$	5.06	6.94	8.28	4.06
$2f_c \pm 3f_{in}$	2.78	2.83	17.25	10.79
$3f_c \pm 3f_{out}$	0.89	0.62	2.92	9.98
$3f_c \pm 6f_{in} \pm 3f_{out}$	3.95	6.45	0.62	1.21
$4f_c \pm 3f_{out}$	6.62	5.06	0.93	3.35
$4f_c \pm 3f_{in}$	0.35	0.33	7.38	1.16
$5f_c \pm 3f_{out}$	0.25	0.34	1.26	0.38
$5f_c \pm 6f_{in} \pm 3f_{out}$	2.82	3.68	0.94	1.09

Comparing Tables 3 and 6, it can be seen that the maximum difference between the theoretical data and experimental data of common-mode components of CMV of method 1 and method 4 is 2.91% when $m = 0.3$. Comparing Tables 4 and 7, it can be seen that the maximum difference between the theoretical data and experimental data of CMV of method 1, method 2, method 3 and method 5 is 3.05% when $m = 0.7$. The deviation is within a reasonable range and does not affect the analysis of results, so the correctness of theoretical analysis is verified by experiments.

5. Conclusions

In this paper, the common-mode spectrum of five modulation methods is obtained by the triple Fourier series. By comparing and analyzing the low-frequency amplitude characteristics and high-frequency amplitude characteristics of five modulation methods, the suppression performance of the five modulation methods is evaluated. Through common-mode spectrum analysis, the following conclusions can be drawn:

1. The common-mode components are mainly concentrated at integer multiples of switching frequency, and the integer multiple switching frequency is symmetrically distributed. The farther away from the switching frequency, the smaller the amplitude of the common-mode components.

2. The higher the frequency, the smaller the amplitude of common-mode components. When frequency reaches $3f_c$ or above, the amplitude of common-mode components is very small.

3. By analyzing the effect of voltage transmission ratio on common-mode components, it can be seen that voltage transmission ratio m has a greater influence on common-mode components of $0{\sim}3f_c$ frequency bands.

4. By comparing and analyzing frequency domain characteristics of common-mode components of five modulation methods, modulation method 1, where the inverter stage uses four effective vectors, has the strongest ability to suppress common-mode components among five modulation methods.

References

1. Wheeler, P.W.; Rodriguez, J.; Clare, J.C.; Empringham, L.; Weinstein, A. Matrix converters: A technology review. *IEEE Trans. Ind. Electron.* **2002**, *49*, 276–288. [CrossRef]
2. Lee, M.; Wheeler, P.; Klumpner, C. Space-vector modulated multilevel matrix converter. *IEEE Trans. Ind. Electron.* **2010**, *57*, 3385–3394. [CrossRef]
3. Ayano, H.; Murakami, K.; Matsui, Y. A Novel Technique for Reducing Leakage Current by Application of Zero-Sequence Voltage. *IEEE Trans. Ind. Appl.* **2015**, *51*, 3094–3100. [CrossRef]
4. Cao, S.; Niu, F.; Huang, X. Time–frequency characteristics research of common mode current in PWM motor system. *IEEE Trans. Power. Electron.* **2020**, *35*, 1450–1458. [CrossRef]
5. Turzynski, M.; Chrzan, P.J. Reducing Common-Mode Voltage and Bearing Currents in Quasi-Resonant DC-Link Inverter. *IEEE Trans. Power Electron.* **2020**, *35*, 9553–9562. [CrossRef]
6. Takahashi, S.; Ogasawara, S.; Takemoto, M.; Orikawa, K.; Tamate, M. Common-Mode Voltage Attenuation of an Active Common-Mode Filter in a Motor Drive System Fed by a PWM Inverter. *IEEE Trans. Ind. Appl.* **2019**, *55*, 2721–2730. [CrossRef]
7. Jayaraman, K.; Kumar, M. Design of Passive Common-Mode Attenuation Methods for Inverter-Fed Induction Motor Drive with Reduced Common-Mode Voltage PWM Technique. *IEEE Trans. Power Electron.* **2020**, *35*, 2861–2870. [CrossRef]
8. Nguyen, T.; Lee, H. Modulation strategies to reduce common-mode voltage for indirect matrix converters. *IEEE Trans. Ind. Electron.* **2012**, *59*, 129–140. [CrossRef]
9. Nguyen, T.; Lee, H. A new SVM method for an indirect matrix converter with common-mode voltage reduction. *IEEE Trans. Ind. Inform.* **2014**, *10*, 61–72. [CrossRef]
10. Padhee, V.; Sahoo, A.; Mohan, N. Modulation techniques for enhanced reduction in common-mode voltage and output voltage distortion in indirect matrix converters. *IEEE Trans. Power Electron.* **2017**, *32*, 8655–8670. [CrossRef]
11. Tsoupos, A.; Khadkikar, V. A novel SVM technique with enhanced output voltage quality for indirect matrix converters. *IEEE Trans. Ind. Electron.* **2019**, *66*, 832–841. [CrossRef]
12. Li, S.; Jin, Z.; Liu, X.; Han, X.; Deng, W. Open-current vector based SVM strategy of sparse matrix converter for common-mode voltage reduction. *IEEE Trans. Ind. Electron.* **2021**, *68*, 7757–7767. [CrossRef]
13. Li, S.; Wang, W.; Han, X. A DPWM modulation strategy to reduce common-mode voltage for indirect matrix converters based on active-current vector amplitude characteristics. *IEEE Trans. Ind. Electron.* **2022**, *69*, 8102–8112. [CrossRef]

14. Wang, H.; Su, M.; Sun, Y. Topology and modulation scheme of a three-level third-harmonic injection indirect matrix converter. *IEEE Trans. Ind. Electron.* **2017**, *64*, 7612–7622. [CrossRef]

15. Jiang, X.; Xiao, X.; Liu, H. The output spectrum analysis of high-power multilevel voltage source converters using double Fourier series. In Proceedings of the Transmission & Distribution Conference & Exposition, Dalian, China, 18 August 2005; pp. 1–5.

16. Li, S.; Xia, C.; Yan, Y. Space-vector overmodulation strategy for ultrasparse matrix converter based on the maximum output voltage vector. *IEEE Trans. Power Electron.* **2017**, *32*, 5388–5397. [CrossRef]

17. Wang, B.; Sherif, E. Analytical characterization of the spectral performance of matrix converters. In Proceedings of the International Power Electronics and Motion Control Conference, Harbin, China, 2–5 June 2012; pp. 678–682.

18. Qiu, L.; Xu, L.; Li, Y. Spectral analysis of a scalar modulated matrix converter based on 3-D Fourier integral. In Proceedings of the European Conference on Power Electronics and Applications, Warsaw, Poland, 11–14 September 2017; pp. 1–8.

19. Shi, T.; Wu, L.; Yan, Y.; Xia, C. Harmonic spectrum of output voltage for space vector-modulated matrix converter based on triple fourier series. *IEEE Trans. Power Electron.* **2018**, *33*, 10646–10653. [CrossRef]

20. Shi, T.; Wu, L.; Yan, Y.; Xia, C. Harmonic spectrum of output voltage for space vector pulse width modulated ultra sparse matrix converter. *Energies* **2018**, *11*, 390. [CrossRef]